

ALPHA SPECTROSCOPY WITH SUPEHEATED EMULSION DETECTORS

T. Morlat^a, A. Kling^a, A.C. Fernandes^a, M. Felizardo^a, T. A. Girard^a, J.G. Marques^a
and F.P. Carvalho^a

^aC²TN, Centro de Ciências e Tecnologias Nucleares, Instituto Superior Técnico, Universidade de Lisboa,
E.N. 10, 2695-066 Bobadela LRS, Portugal

Abstract

In this work we demonstrate that Superheated Emulsion Detectors (SEDs) have the capacity to be used in α -spectroscopy of liquid sources with very low activities. Experimental data for three different Th radionuclides with α energies ranging from 4 to 6 MeV could be clearly distinguished by ramping up the operational temperature of the SEDs. The experimental results are analyzed via a recently introduced α – droplet interaction model.

1. INTRODUCTION

Superheated Emulsion Detectors (SED) consist of millions of micrometer-sized droplets in a superheated state embedded in a compatible gel matrix. Particles with both, an energy and a linear energy transfer (LET) above thermodynamically defined critical limits, passing through a droplet cause it to evaporate and grow into a gas bubble. The acoustic signal that accompanies the explosive growth of the bubble can be detected with a microphone. Further, acoustic signals arising from alpha-particles and nuclear recoils caused by fast neutron scattering can be distinguished based on their amplitudes.

Alpha spectrometry at very low activity levels (far below 1 Bq) is of highest interest for several applications. For example, alpha emitters in electronic circuits can cause soft errors critical in many applications [Kob2009, Fer2016]. With decreasing circuit sizes and higher purity conventional alpha counting methods are no more applicable. SEDs also offer a method to detect alpha-emitters with extremely low intensity gamma transitions at very low activity levels (e.g. ²⁴⁰Pu). Another potential application is a sensitive and easy method for the detection of highly radiotoxic alpha emitters in liquids with simultaneous presence of large amounts of beta- and gamma-emitters, as demanded in nuclear accident conditions [Bu2014, Mor2019]. In this case, the insensitivity of SEDs to beta- and gamma radiation is a highly desirable asset enabling measurement of liquids without preprocessing.

Although the ability of alpha particles to cause a phase transition in superheated liquids is known for a long time [Hah1961], up to now no experimental proof of alpha spectrometry using this effect has been presented. Kozynets et al. [Koz2019] suggest that alpha particles with different energies can be distinguished by the acoustic power of bubble expansion in the case of SEDs loaded with C₃F₈.

1 In a previous work [Mor2020] the response of C₂ClF₅-based SEDs to the actinide uranium and the rare
2 earth samarium have been studied. A geometric model of the interaction of alpha particles with the
3 detector material and its relation with the count rates observed has been developed assuming that
4 actinides as well as the chemical related rare earths are trapped at the interface between the droplet and
5 the surrounding gel matrix [Pan1999]. Alpha particles released in the decay are expected to enter into
6 the superheated droplet with high probability. For droplets of a sufficient size alpha particles reach
7 critical LET within the droplet and trigger bubble formation.

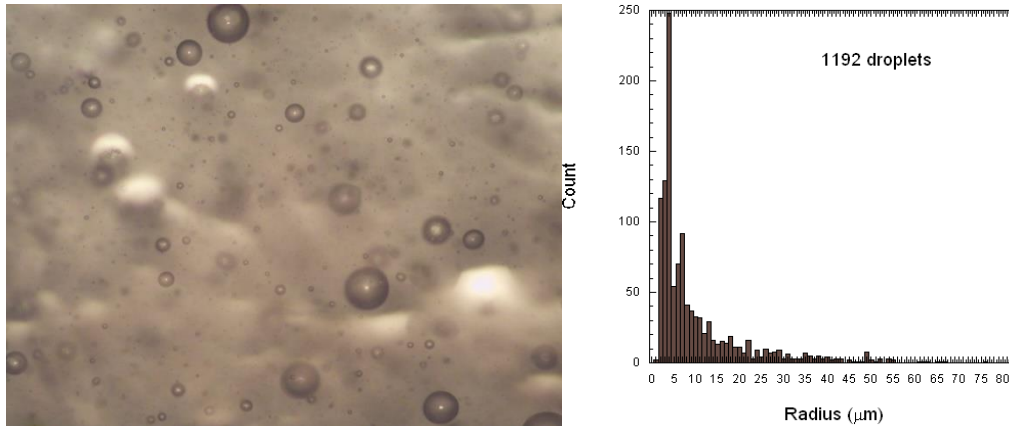
8 The model also predicts that for alpha particles with a given energy bubble growth can only occur above
9 a certain temperature. Consequently, it should be possible to distinguish different alpha emitters by
10 ramping up the temperature of the SED. To test the validity of this assumption we study in this paper
11 the temperature dependence of the SED response to the three naturally occurring thorium radioisotopes:
12 ²³²Th and ²²⁸Th from the thorium decay series and ²³⁰Th from the ²³⁸U decay chain.

13 **2. EXPERIMENTAL**

14 **2.1 Detector fabrication protocol**

15 For the investigations 150 ml SED containing 2.0 - 5.9 g of C₂ClF₅ were produced using the following
16 protocol: The detector gel is prepared by mixing gelatin, PolyVinylPyrrolidone (PVP), bidistilled water
17 and glycerin as described in Ref [Mor2020]. On the following day 100 µl (0.37 Bq ²³²Th) or 1 ml (3.7
18 Bq ²³²Th) of a thorium liquid source (thorium nitrate, ICP standard grade, 1.000±0.007 g l⁻¹) is injected
19 into the gel kept at 44 °C. The activities of the relevant alpha-emitting radioisotopes in the solutions
20 were verified by α-spectrometry (ORTEC-EG&G OCtetePlus with 450 mm² surface barrier detectors);
21 the measured element concentration agreed with the nominal value within ± 4%. The detector material
22 is agitated vigorously before being placed inside the hyperbaric chamber. For the formation of the
23 detector emulsion, the mixture is continuously stirred (300 rpm) for 4 h at a pressure of 20 bar and a
24 temperature of 44 °C. The heating is then turned off to let the emulsion cool down and the stirring is
25 reduced to 50 rpm. After one hour further cooling to 5 °C is initiated using a cold water circulation
26 system. 12 hours later the pressure in the chamber is gradually lowered to ambient pressure and the SED
27 taken out for use.

28 For the determination of the droplet size distribution (DSD) in the SED some from slices of gel are taken
29 from randomly chosen positions. Droplet sizes are determined from pictures taken with an optical
30 microscope (Zeiss, Axio Lab A1). A typical DSD with 1 µm bin size is shown in Fig. 1 (right), peaking
31 at a droplet radius (R) of 4 µm and an average of 5 µm, and never exceeding 50 µm. In the following
32 the DSD is assumed to be a Lorentzian with an expected value centered at 5 µm and a width $\Gamma = 4 \mu\text{m}$.



1
2 Figure 1. On the left, a picture of superheated droplets in the gel made by optical microscopy. The mean radius is $5\mu\text{m}$ and
3 the mean inter-droplet distance between two closest droplets is $\langle d_{gel} \rangle = 42\mu\text{m}$. On the right the DSD based on 1192 droplets
4 is shown.

5
6 **2.2 Acoustic instrumentation and measurement set-up**

7
8 Each SED is equipped with a top-mounted MCE-200 Panasonic microphone with a frequency range of
9 $0.020\text{--}16\text{ kHz}$ (3dB). The read-out and signal processing instrumentation is identical with that of the
10 dark matter search experiment SIMPLE [Fel2014]. The recorded acoustic signals are processed using a
11 MatLab-based digital band-pass filter for frequencies of $100\text{--}300\text{ Hz}$ and applying a threshold of 0.2 mV
12 for the signals to suppress the noise.

13
14 A Th-doped SED is placed together with an undoped reference SED for background determination
15 inside a bath with circulating water which temperature is kept at constant temperature using a
16 refrigerating unit (Huber, TC45E) and a polystat heating immersion circulator (Cole Parmer, 12120). A
17 temperature probe (IKA-Werke, PT 100) placed in the reference SED monitors the actual detector
18 temperature.

19
20 The SED with 3.7 Bq activity was measured directly after fabrication. For the other SEDs with lower
21 activity (0.37 Bq) the measurement campaigns were started one, three and six days after the fabrication
22 in order to study the long-term behavior of the SEDs. The detectors were stored at $3\text{ }^\circ\text{C}$ and 98000 Pa in
23 order to avoid radiation-induced nucleations.

24
25 For all SEDs measurements were performed ramping up the temperature from $5\text{ }^\circ\text{C}$ to $13\text{ }^\circ\text{C}$ in steps of
26 $1\text{ }^\circ\text{C}$. At each temperature, after reaching equilibrium, signals were accumulated for 20 minutes for both,
27 the Th-doped and the reference SED.

28
29 **3. MODEL-BASED PREDICTIONS**

1 The conditions for bubble nucleation under particle irradiation are given by the Seitz model [Sei1958]:

$$2 \quad E \geq E_c = 4\pi R_c^2 \left(\sigma - T \frac{\partial \sigma}{\partial T} \right) + \frac{4\pi}{3} R_c^3 \rho_v h_v - \frac{4\pi}{3} R_c^3 \Delta P \quad , \quad (1)$$

3 and the deposition must occur within a critical track length,

$$4 \quad dE/dx \geq E_c/L_c \quad , \quad (2)$$

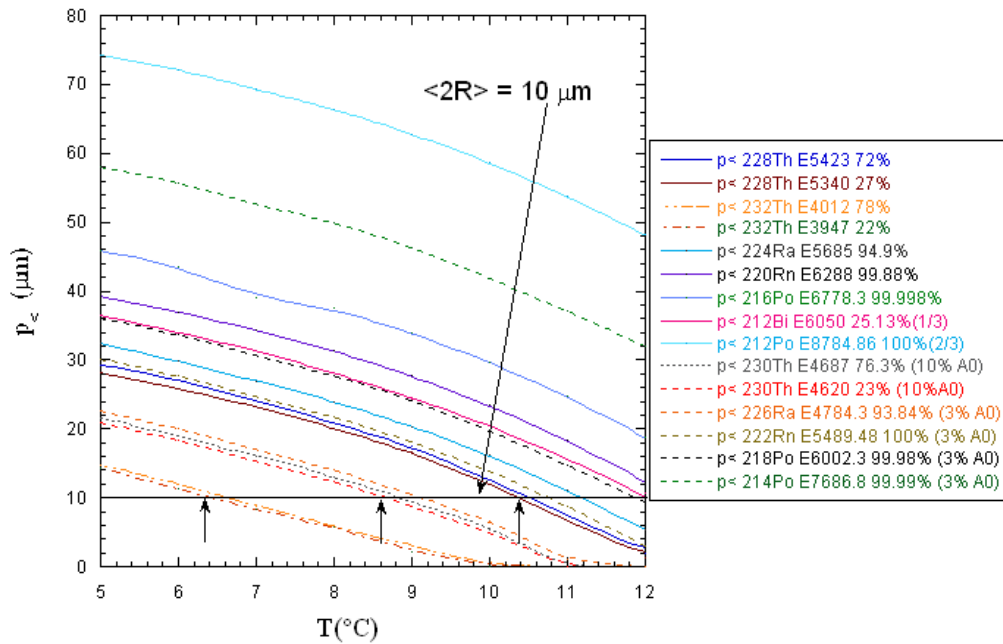
5 where T is the SED operating temperature, σ the surface tension of the bubble, ρ_v the vapour density,
6 $h_v(T) = h_l - h_v$ the heat of vaporization. $R_c = 2\sigma(T)/\Delta P$ where $\Delta P = P_v - P_l$ is the difference pressure between
7 the vapour P_v and liquid P_l . The E_c/L_c is the critical linear energy transfer (LET_c), required for bubble
8 nucleation, with $L_c = \Lambda R_c$ being the effective ionic energy deposition length, and Λ a liquid-dependent
9 parameter: $\Lambda(T, P)$ with P being the operation pressure [14, 8, 9].

10 The model introduced in Ref. [Mor2020] is based on the intersection of two spheres: one, the
11 superheated droplet, and the second, a sphere of radius $p_<$ which defines the penetration distance of the
12 α -particle in the droplet necessary to achieve LET_c. Since the size of the intersection depends on the
13 relation between $p_<$ and the droplet size, different droplet radii exhibit a different nucleation probability.

14 **3.1 Minimum depth penetration $p_<$ versus temperature**

15 A solution made of chemically purified natural thorium is expected to contain the primordial α -emitting
16 radioisotope ^{232}Th and its descendent ^{228}Th in secular equilibrium. The other alpha emitters from the
17 thorium decay chain had been removed in the chemical purification process but reestablished
18 equilibrium with ^{228}Th due to their short half-lives. A third naturally occurring thorium radioisotope to
19 be considered is ^{230}Th ($T_{1/2} = 7540$ y), a descendent of ^{238}U , although the parent uranium has been
20 chemically removed from the solution. Due to the considerable half-lives of ^{230}Th and its α -emitting
21 daughter ^{226}Ra ($T_{1/2} = 1630$ y) an equilibrium in the remaining decay chain is established. For the solution
22 used in this work (aged 4 years) the activity of ^{226}Ra and its descendants contribute only with a few
23 percent relative to ^{230}Th .

24 In total, 11 different alpha emitters with 15 major alpha energies can be identified and the corresponding
25 Bragg curves for superheated C_2ClF_5 in the 5 to 12 °C temperature range were computed using SRIM-
26 2008 [SRIM2008]. The minimum depth penetration ($p_<$) is then given by the depth at which the
27 calculated stopping power reaches LET_c. Applying the relation $\Lambda(T) = 4.3(\rho_l/\rho_v)^{1/3}$, with ρ_l being the
28 liquid density, the dependence of the minimum depth penetration ($p_<$) on the temperature (at fixed
29 pressure) can be determined. Figure 2 shows the dependence of $p_<$ on the temperature of the refrigerant
30 at 98000 Pa. The temperatures at which $p_< = 10$ μm , i.e., equivalent to the average droplet diameter of
31 the SDDs used in this work can be easily extracted from this plot.



1

2 Figure 2. Minimum penetration depth ($p_{<}$) required to achieve LET_c for several α emitters from the Thorium chain (α 's of
3 energy E and % isotopic abundance), as a function of temperature (T) and at 98000 Pa pressure.

4 For the thorium radioisotopes the threshold temperatures at which they contribute to the counting rate
5 by causing nucleation are 6 °C (²³²Th, 3.9 and 4.0 MeV), 8 °C (²³²Th, 4.6 and 4.7 MeV) and 10 °C (²²⁸Th,
6 5.3 and 5.4 MeV). In case radium adheres to the droplet surface, the contributions of its isotopes have
7 to be considered. ²²⁴Ra is expected to show an effect at temperatures above 11.5 °C which is at the limit
8 of the experimental temperature range since the refrigerant C₂ClF₅ in superheated state starts to be
9 sensitive to γ -ray induced nucleation at 13 °C. On the other hand, ²²⁶Ra with its threshold of about 6.5
10 °C and will probably overlap with the ²³⁰Th contribution.

11 Radon, being a chemically inert noble gas, is expected to diffuse freely through the detector volume
12 rather than to adhere to the droplet surface. Radon nuclei disintegrating in the gel are likely to be stopped
13 before encountering a droplet. On the other hand, an alpha from a radon nucleus decaying at a random
14 position and direction within a droplet will most likely leave it without causing a nucleation. Only the
15 15% of the droplets which have a radius above 20 μm could suffer a nucleation due to the decay of
16 ²²²Rn. The remaining isotopes from the thorium decay sequence ²¹²Po, ²¹⁶Po, ²¹²Bi and ²²⁰Rn show
17 threshold temperatures above 12 °C and can be discarded for this study.

18 Since about 50 % of the bubbles have diameters between 8 and 12 μm a first estimate of the energy
19 resolution of the detector can be obtained by determining the difference between temperatures ΔT for
20 these values of $p_{<}$. For the radioisotopes of interest $\Delta T = 1.2$ °C, 0.9 °C and 0.8 °C for ²³²Th, ²³⁰Th and
21 ²²⁸Th, respectively. These values are clearly smaller than the interval between the temperatures at which
22 $p_{<} = 10$ μm is attained for the three Th isotopes. Therefore, it is expected that a measurement in steps of
23 1 °C will allow to distinguish them.

1 3.2 Event rate

2 Applying the model developed in [Mor2020] it is possible to estimate the event rate, $\tau_{\alpha}^{surface}$, given
 3 by:

$$4 \quad \tau_{\alpha}^{surface}(T \leftrightarrow p_{<}) = \frac{1}{2} A_0 \varepsilon_{att} \sum_{k_{\alpha}} f_{k_{\alpha}} \varepsilon(p_{<}) F(p_{<})$$

5 where A_0 the activity, ε_{att} acoustic attenuation factor due to bubble formation (see [Mor2020] for details),
 6 $f_{k_{\alpha}}$ the probability of an alpha transition with a certain energy occurring for the decay of the isotope k,
 7 $\varepsilon(p_{<})$ the average nucleation efficiency (calculated for each temperature and all involved droplet sizes),
 8 and $F(p_{<})$ the "number of droplets" efficiency, i.e., the number of droplets that nucleate at each
 9 temperature.

10 Using the bubble nucleation efficiency, ε_{nuc} ,

$$11 \quad \varepsilon_{nuc}(p_{<}; R) = 1 - \left(\frac{p_{<}}{2R}\right)^2 - 2 \left(\frac{p_{<}}{2R}\right)^3 \left(1 - \frac{p_{<}}{2R}\right)^2 \left(2 + \frac{p_{<}}{2R}\right)$$

12 yields for $\varepsilon(p_{<})$

$$13 \quad \varepsilon(p_{<}) = \frac{\int_{p_{<}/2}^{100} \varepsilon_{nuc}(p_{<}; R) L(R; \Gamma) dR}{\int_0^{100} L(R; \Gamma) dR}$$

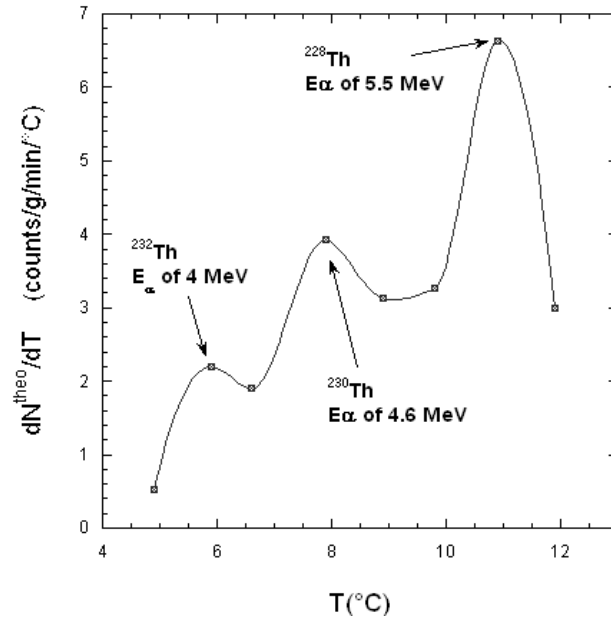
14 where $L(R; \Gamma)$ is the Lorentzian function of width Γ .

15 $F(p_{<})$ corresponds to the area beneath the droplet distribution above which nucleation begins:

$$16 \quad F(p_{<}) = \frac{\int_{p_{<}/2}^{100} L(R; \Gamma) dR}{\int_0^{100} L(R; \Gamma) dR}$$

17 The attenuation factor can be estimated from Fig. 11(b) of Ref. [Mor2020] for each experimental run.

18 As an example the event rate based for 0.3 Bq Th-activity without attenuation is computed and the
 19 resultant differential event rate, i.e., the change in event rate when increasing the temperature, is
 20 represented in Fig. 3. As expected from the qualitative discussion in Sec. 3.1 the main contributors in
 21 the temperature range from 4 to 12 °C are, by increasing energy, ^{232}Th , ^{230}Th and ^{228}Th .



1

2 Figure 3. Calculated differential spectrum assuming an activity of 0.3 Bq ^{232}Th and ^{228}Th , and 0.03 Bq for ^{230}Th . The three
3 peaks show the contribution of the different alpha energies involved. The line is to guide the eyes.

4

5

6 4. RESULTS & DISCUSSION

7 Alpha spectroscopy of the Th liquid source allowed to identify ^{232}Th , ^{228}Th and descendants (^{224}Ra ,
8 ^{220}Rn , ^{216}Po , ^{212}Po , etc.) with identical (equilibrium) activities. Additionally, ^{230}Th and its descendant
9 ^{226}Ra were detected, with activities relative to that of ^{232}Th amounting 10 % and 3 %, respectively. Table
10 1 shows the measured isotopic activities and mass concentrations.

11 Table 1. Measured activity and mass concentration of selected isotopes detected in the thorium solution
12 by α spectrometry.

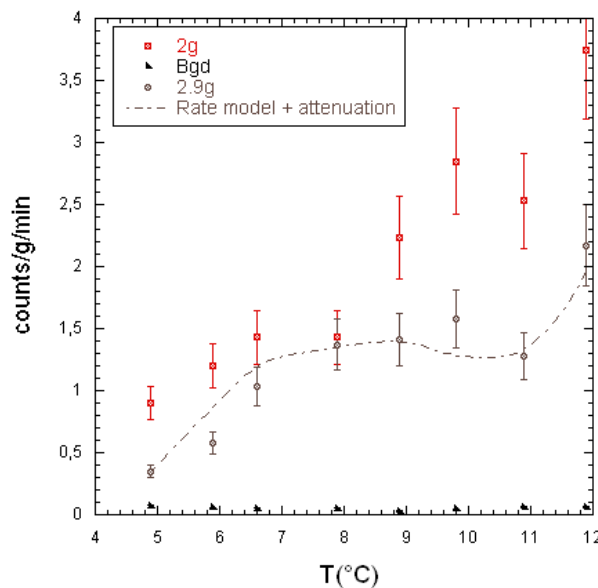
Isotope	Activity concentration (Bq/L)	Mass concentration (g/L)
^{232}Th	$3669 \pm 223 (A_0)$	0.904 ± 0.054
^{230}Th	$364 \pm 36 (10\% A_0)$	$(0.477 \pm 0.04) \times 10^{-6}$
^{228}Th	$3727 \pm 226 (A_0)$	1.22×10^{-10}
^{226}Ra	$117 \pm 20 (3\% A_0)$	3.2×10^{-9}

13

14 4.2 Measurements 1 day after fabrication

1 The measured counting rate vs. temperature for a 2.9 g C₂ClF₅ SED doped with 0.37 Bq Th is plotted
 2 in Fig. 4. The respective theoretical prediction including acoustic attenuation due to pre-existing bubbles
 3 is added demonstrating good agreement with measurements. Increasing the temperature from 5 °C to
 4 6.6 °C results in a strong increase of the count rate since the SED becomes sensitive to the alpha particles
 5 from the ²³²Th decay. The count rise at 7.9 °C is less pronounced as expected due to the lower combined
 6 activity of ²³⁰Th and ²²⁶Ra (about 13% of that of ²³²Th) Nevertheless, the observed increase is larger than
 7 expected. The last steep rise in the count rate curve between 11 and 12 °C can be attributed to ²²⁸Th.

8 Based on the count rate at 12 °C of about 2.15±0.30 cts/g/min and the assumption that the summed
 9 activity of all Th isotopes and ²²⁶Ra (0.79 Bq) contribute to this signal the detection efficiency of this
 10 2.9 g SED can be estimated to be about in the order of 0.1 cts/s/Bq (i.e. 10%).

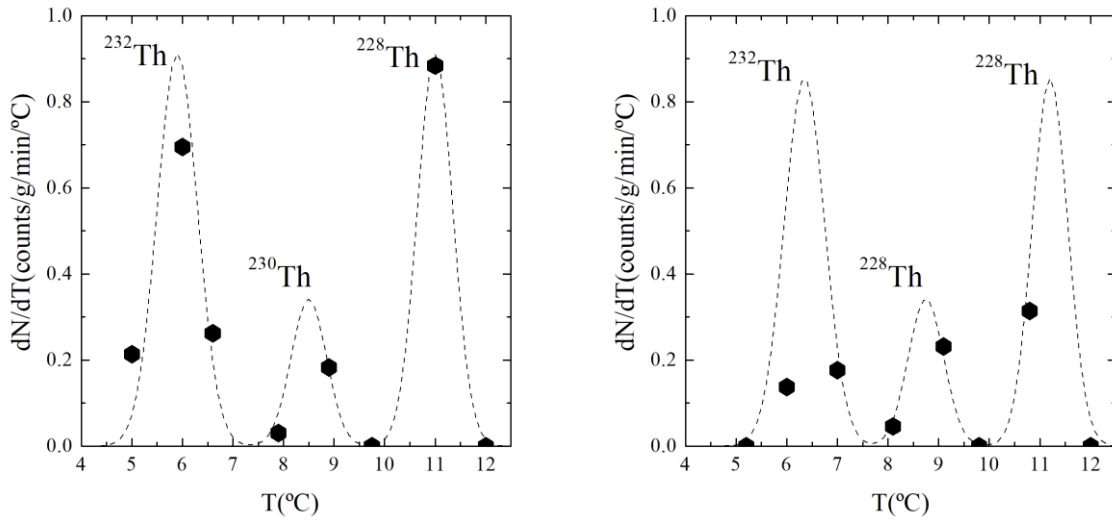


11
 12 Figure 4. Counting rate for two SEDs: {2.0 g; 0.3 Bq Th} in red squares and {2.9 g; 0.3 Bq Th} in grey circles versus
 13 temperature. The background measurements is showed in black triangles. The dotted line represents the model computed
 14 with attenuation.
 15

16 Plotting the change in count rate per temperature unit (dN/dT) rather than the count rate itself in Fig. 5
 17 (left) against the temperature reveals the peaks related to the different isotopes. Gaussian curves are
 18 added to the plots to mimic a differential spectrum obtained using smaller temperature steps. A striking
 19 feature of the experimental results in comparison to the theoretical prediction (Fig. 3) is that dN/dT
 20 reaches or closely approaches zero between the peaks indicating a better energy resolution than
 21 anticipated (Sec. 3.1), amounting to a the full width at half maximum (FWHM) in the order of 0.3 MeV
 22 or 7-8%.

23 An additional SED (2.4 g; 0.37 Bq) was made to confirm the results of 2.9 g SED, its differential
 24 spectrum plotted in Fig. 5 (right). The small shift of the ²³⁰Th peak to a temperature between the

1 measuring points of 6 and 7 °C attributed to a slightly different DSD (a larger fraction of small droplets
 2 enhances sensitivity to low-energy alphas). Using the data obtained in this work and for uranium ^{234}U
 3 and ^{238}U from Ref. [Mor2020] it is possible to establish an apparently linear relationship between the
 4 temperature at which dN/dT is peaking and the energy of the detected alpha particles as depicted in Fig.
 5 6, i.e., a calibration curve. Also included is the presumable location of ^{226}Ra (present in the injected
 6 solution) which has an alpha energy very similar to that of ^{230}Th and therefore will overlap with it in the
 7 experiment.



8

9 Figure 5. Differential spectrum for SEDs doped with 0.3 Bq ^{232}Th and with active masses of 2.9 g (left) and 2.4 g (right)
 10 versus temperature. The three peaks show the contribution of alpha energies of 4 MeV at around 6 °C, 4.7 MeV at 9 °C and
 11 5.5 MeV at 11 °C. Overlaid are Gaussian curves to indicate the temperature dependence.

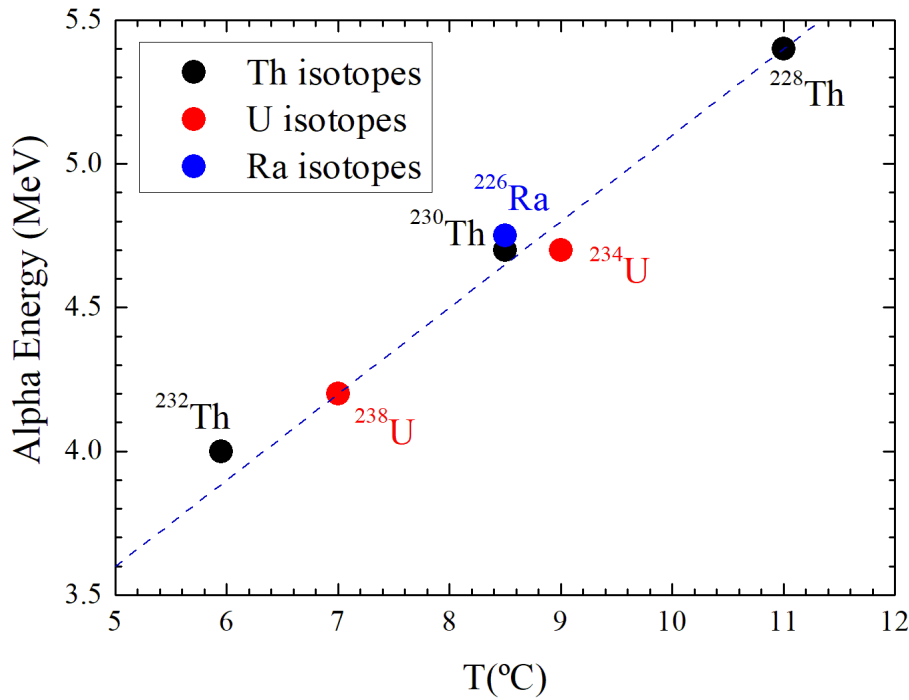
12 The conversion relation between peak temperature and alpha energy is

$$13 \quad E_{\alpha}(\text{MeV}) = 2.1 \text{ MeV} + 0.3 \frac{\text{MeV}}{^{\circ}\text{C}} T$$

14 or the inverse

$$15 \quad T(^{\circ}\text{C}) = -7.9^{\circ}\text{C} + 3.5 \frac{^{\circ}\text{C}}{\text{MeV}} E_{\alpha}$$

16 An extrapolation using this linear fit to ^{147}Sm with an alpha energy of 2.25 MeV indicates that the onset
 17 for the detection of this radionuclide is located at about 0.5 °C which explains the observation of a
 18 constant event rate above 5 °C in samples doped with this radionuclide as observed in [Mor2020].



1

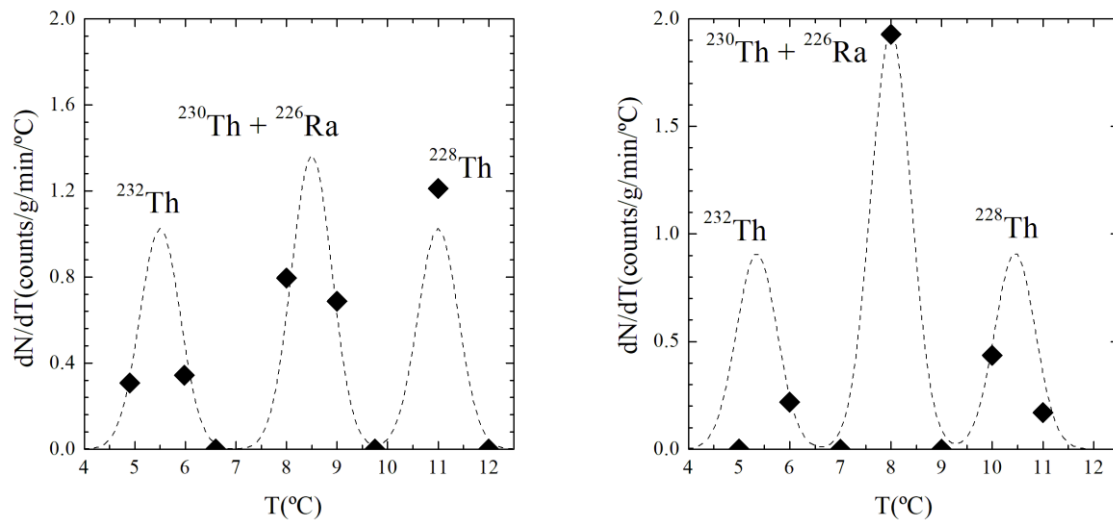
2

Figure 6. Relationship between peak temperature and alpha energy in the SDD.

3 4.3 Measurements 4 and 7 days after fabrication

4 In order to study the influence of the time elapsed between the detector fabrication and the actual
 5 measurement series two detectors doped with 0.37 Bq Th were measured after four and seven days
 6 resting time, respectively.

7 The differential spectrum of a 2.0 g SED, acquired 4 days after fabrication, is displayed in Fig. 7 (left):
 8 the peak locations related to ^{232}Th (between 5 and 6 °C) and ^{230}Th (between 8 and 9 °C) appear in this
 9 case at slightly lower temperature than expected. Since 4 days elapsed between the detector preparation
 10 and the measurements it is likely that a part of the smaller droplets underwent Ostwald ripening forming
 11 larger ones. This process shifts the DSD towards a larger average size and consequently the detection
 12 onset to lower temperatures. . Moreover, an increase of the $^{230}\text{Th}+^{226}\text{Ra}$ to ^{232}Th peak height ratio is
 13 observed with respect to measurements after one day.



1

2 Figure 7. Left: differential spectrum for 2.0 g SDD (0.3 Bq Th) versus temperature after 4 days and right: 5.8 g SDD after 7
 3 days with the respective peak identifications and overlaid Gaussian curves.

4

5 Figure 7(right) shows the spectrum for a 5.8 g detector acquired 7 days after fabrication . The most
 6 striking feature is a further increase of the $^{230}\text{Th}+^{226}\text{Ra}$ relative to the main constituents ^{232}Th and ^{228}Th .

7 A similar strong enhancement of the count rate over the expected value after ^{226}Ra injection in a C_4F_{10} -
 8 containg SED has been observed by Aubin [Aub07]. Archambault et al. [Arc2011] report a quantitative
 9 result for the same type of SED stating that the nucleation rate for ^{226}Ra is 47 higher than for ^{241}Am
 10 when measured two weeks after the production.

11 This effect can be attributed to the migration of ^{226}Ra to the gel-droplet interface during the waiting time
 12 between production and measurement. The higher affinity of radium to the interface with regard to
 13 americium, thorium and very likely uranium can be attributed to differences in their chemistry. Radium
 14 as the most water-soluble of all alkaline earth metals is expected to be initially fully dissolved in the gel
 15 matrix. During diffusion, it becomes trapped at the interface with the droplet which seems to offer an
 16 energetically preferable environment. On the other hand, the hydrophobic character of actinides (such
 17 as thorium, uranium and americium) prompts a stable population at the droplet interface but presumably
 18 with less affinity than radium.

19 4.4 Measurements at high exposure (3.0 Bq Th)

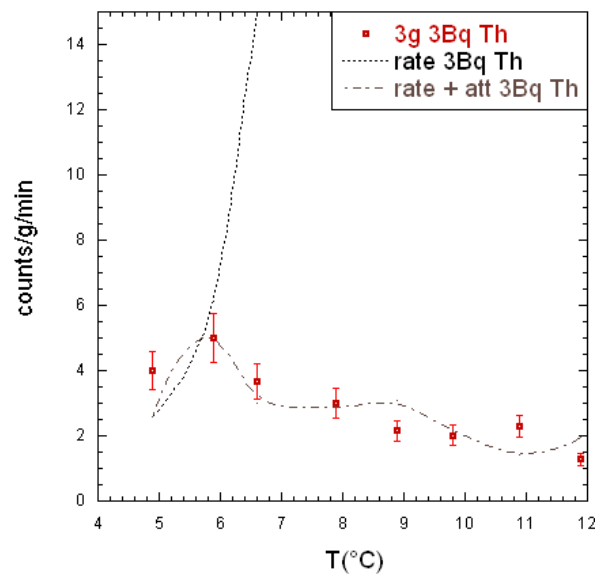
20 The SED response to larger activity concentrations was investigated in order to assess its performance
 21 in a challenging situation of intense bubble formation and accumulation. For this purpose an activity
 22 one order of magnitude larger (3.0 Bq) than in the previous cases has been injected while the active
 23 detector mass was virtually the same (3 g). Measurements were started directly after fabrication.

1 Figure 8 presents the counting rates observed with 3.0 Bq ^{232}Th . At the beginning of the measurement
 2 ($T = 5^\circ\text{C}$) a counting rate of 4 cts/g/min was observed, in good agreement with the theoretical value of
 3 2.6 cts/g/min. However, and in contrast to measurements with lower activities, the expected increase of
 4 the count rate with temperature is not observed. As discussed in [Mor2020], this effect can be attributed
 5 to the attenuation of the acoustic signal induced by (and outweighing) the much larger number of bubbles
 6 produced at each temperature. Table 2 includes the attenuation efficiencies calculated from the power
 7 laws derived in [Mor2020] and, together with Figure 8, demonstrates how their inclusion into the
 8 theoretical prediction effectively describes the experimental data.

9 Table 2. Results of 3 Bq Th with attenuation efficiency (3 g active mass). R_{0t} represents the calculated
 10 number of events without attenuation, τ^{att} the theoretical count rate corrected for signal attenuation and
 11 τ^{meas} the observed count rate, both in units of counts per gram and minute.

$T(^{\circ}\text{C})$	5	6	7	8	9	10	11	12
R_{0t}	1092	2364	5964	14580	33060	59124	92868	151572
ϵ_{att}	1	1	0.2	0.08	0.04	0.02	0.01	0.008
τ^{att}	2.6	5.2	3	2.87	3.08	2.16	1.4	1.95
τ^{meas}	4	5	3.67	3	2.15	2.02	2.30	1.28

12



13

14 Figure 8. The counting rates for a 3 g active mass SDD with 3 Bq ^{232}Th versus temperature (red squares). The dotted line
 15 shows the theoretical rate expected without and the dotted line with the attenuation [Mor2020].

16

1 5. CONCLUSIONS AND OUTLOOK

2 In this paper the ability of C₂ClF₅-based SEDs to clearly discriminate alpha particles of various energies
3 by varying the detector temperature within a relatively small temperature range has been demonstrated
4 using Th and Ra isotopes. This study complements and confirms previous measurements using U and
5 Sm isotopes [Mor2020] evidencing the applicability of SEDs in the alpha spectrometry in the range
6 below 1Bq.

7 Important characteristics for the use in alpha-spectrometry as the energy-temperature calibration,
8 attainable energy resolution, detector efficiency, influence of delayed measurement and influence of
9 activity introduced were studied. As expected the SED works best shortly after production and with very
10 low activities showing its potential for environmental and accident applications.

11 Clearly, the droplet size distribution is critical for detector performance since small deviation in the
12 average size will induce an alteration of the temperature-energy dependence. Future work will focus on
13 the development of monosized droplets allowing to control the detector response and improve its energy
14 resolution. A further aim is the extension of the detection energy range by adjusting the droplet size and,
15 if necessary, use of other refrigerants.

16 Acknowledgements

17
18 We thank Dr. José Vieira Antunes for helpful discussion regarding the acoustic attenuation. This work
19 was funded by projects IF/00628/2012/CP0171/CT0008, UID/Multi/04349/2013 and PTDC/EEI-
20 ELC/2468/2014 of the Portuguese Foundation for Science and Technology (FCT).

21 22 References:

- 23 [Kob2009] H. Kobayashi, N. Kawamoto, J. Kase, et al., *Alpha Particle and Neutron-induced Soft Error*
24 *Rates and Scaling Trends in SRAM*, Proc. 2009 IEEE Intl. Reliability Physics Symp., (2009) 206.
25
26 [Fer2016] A.C. Fernandes et al., *Detection of Alpha Particle Contamination in ULA Grade Integrated*
27 *Circuits*, E3S Web of Conferences **12** (2016) Art. No. 03004
28
29 [Bu2014] W. Bu et al., *Release of Pu Isotopes from the Fukushima Daiichi Nuclear Power*
30 *Plant Accident to the Marine Environment Was Negligible*, Environ. Sci. Technol. **48** (2014) 9070
31
32 [Mor2019] Y. Morishita et al., *Detection of Alpha Particle Emitters Originating from Nuclear Fuel*
33 *Inside Reactor Building of Fukushima Daiichi Nuclear Power Plant*, Scientific Rep. **9** (2019) Art. No.
34 581
35
36 [Hah1961] B. Hahn, *The Fracture of Liquids under Stress Due to Ionizing Particles*, Il Nuovo
37 Cimento **22** (1961) 650
38
39 [Koz2019] T. Kozynets, S. Fallows, C. B. Krauss, *Modeling emission of acoustic energy during bubble*
40 *expansion in PICO bubble chambers*, Phys. Rev. D **100** (2019) Art. No. 052001

1
2 [Mor2020] T. Morlat et al., *Response of Superheated Emulsion Detectors to low energy alpha*
3 *irradiation*, Nucl. Instr. Meth. **A 953** (2020) Art. No. 163124
4
5 [Pan1999] L.K. Pan, C.-K.C. Wang, *Superheated-liquid-droplet technique for measuring alpha decays*
6 *in uranium solutions*, Nucl. Instr. Meth. **A 420** (1999) 345
7
8 [Sei1958] F. Seitz, *On the Theory of the Bubble Chamber*, Phys. Fluids 1 (1958) 2

9 [Fel2014] M. Felizardo et al., *Phase II of the SIMPLE Dark Matter Search*, Phys. Rev. D **89** (2014) Art.
10 No. 072013

11 [SRIM2008] <http://www.srim.org/SRIM/>

12 [Aub2007] F. Aubin, *Caractérisation spatiale des événements dans les détecteurs PICASSO*, PhD
13 thesis, Université de Montréal, 2007

14 [Arc2011] S. Archambault et al., *New insights into particle detection with superheated liquids*, New J.
15 Phys. **13** (2011) Art. No. 043006